Journal of Biomedical Materials Research Part A

WILEY

Society For Biomaterials

RESEARCH ARTICLE OPEN ACCESS

In Vitro Evaluation of Periodontal Fibroblast Response to Bioinspired Porous Channel-Embedded Zirconia Surfaces

Joana Ribeiro[1] | Manuela Proença[1] | Flávio Rodrigues[1] | Diego Chaves[2] | Diana P. Ferreira[2] | Lia Rimondini[3] | Michael Gasik[4] | Filipe S. Silva[1,5] | Sara Madeira[1,5]

[1]Center for Micro-Electro Mechanical Systems (CMEMS-UMinho), University of Minho, Guimarães, Portugal | [2]Centre for Textile Science and Technology (2C2T), Textile Engineering Department, University of Minho, Guimarães, Portugal | [3]Center for Translational Research on Autoimmune and Allergic Disease, CAAD, Department of Health Sciences, Università del Piemonte Orientale, Novara, Italy | [4]Department of Chemical and Metallurgical Engineering, School of Chemical Engineering, Aalto University Foundation, Aalto, Espoo, Finland | [5]LABBELS—Associate Laboratory, Braga, Guimarães, Portugal

Correspondence: Sara Madeira (saramadeira@dem.uminho.pt)

Received: 26 August 2025 | **Revised:** 8 March 2026 | **Accepted:** 17 March 2026

Keywords: bioinspired surfaces | channels | fibrointegration | porous structure | zirconia

ABSTRACT

Customized implant approaches are emerging to meet specific patient needs while minimizing complications. Despite advances in osseointegrated implants, issues such as excessive bone loading, bacterial infiltration, peri-implantitis, and bone loss persist. Bioinspired designs with customized geometries and surfaces that promote fibrointegration, inspired by the periodontal ligament of a natural tooth, are increasingly recognized as a promising strategy. This study aimed to evaluate the ability of bioinspired zirconia surfaces to promote adhesion and guide the orientation of human periodontal ligament fibroblasts (hPLFs). Zirconia specimens with internal microchannels and an external porous coating were designed to mimic dentinal tubules and cementum-like features. Fabrication was performed using CAD/CAM CNC milling, followed by dip coating with zirconia suspensions. Microstructural characterization was carried out using scanning electron microscopy (SEM). hPLFs were cultured on the surfaces under a medium gradient (2% vs. 10% FBS) to induce migration from the porous exterior toward the channeled interior. Electrical impedance spectroscopy (1–100 kHz, Gamry system) was used to complement cell viability results and to better understand fibroblast behavior, considering the combined contributions of the cell layer, the culture medium, and the electrode-electrolyte interface. Specimens with 322 ± 7.86 μm channels and porous coatings (167.04 ± 51.87 μm thickness, 9% porosity) were produced. All were biocompatible, with the highest proliferation observed on specimens combining channels and porosity. SEM analysis revealed fibroblasts embedded within the porous layer, with spindle-like extensions anchoring and extending toward channels. Channel-porous specimens also exhibited the highest impedance after 3 days, suggesting enhanced attachment, migration, and spreading. These findings indicate that channel-porous zirconia surfaces enhance fibroblast adhesion and spreading in vitro, supporting their potential to guide structured cell organization. This bioinspired design represents an initial proof of concept for improving soft tissue interactions at the implant interface, paving the way for future fibrointegrative implant concepts such as root-analogue dental implants.

1 | Introduction

The World Health Organization (WHO) estimates that oral diseases affect nearly 3.5 billion people worldwide [1] with tooth loss being one of the leading causes of this burden [1]. The osseointegrated dental implants, in which the implant directly contacts the surrounding alveolar bone [2] through a rigid connection established by new bone formation around the implant

surface, are the current practice to replace missing teeth [3]. These implants lack periodontium structures such as cementum, the outermost hard tissue layer of the tooth, and periodontal ligament (PDL), which are essential for natural biomechanics, shock absorption, sensory function, and bacterial protection. Consequently, the absence of these structures results in clinical challenges such as implant loosening, high pressures of mastication due to their lack of mechanical stability and shock absorption, no sensory information in the mastication system, and peri-implantitis [4, 5].

In addition to this issue, the osseointegrated implants are commonly composed of titanium (Ti) and its alloy (Ti6Al4V). The inertness of Ti has been questioned in the last years [6], as a metal can undergo corrosion, releasing Ti particles into the bloodstream [6] which can lead to allergic reactions and it is unesthetic due to its gray color, especially when gingiva regression occurs. Zirconia (ZrO_2), a ceramic material, is a potential alternative to overcome the Ti drawbacks. It is aesthetically pleasing, with a tooth-like color, inert, biocompatible and has a minor propensity for bacterial adhesion and biofilm formation on its surface [7], making it a great potential material for dental implants [8]. In terms of design, these conventional implants are typically cylindrical or tapered with threaded designs, offer limited customization and require invasive procedures such as bone drilling, sinus lifting, and bone augmentation, often causing patient discomfort and longer recovery. Poor fit between the implant and bone socket can lead to stability loss and implant failure. Viable design alternatives are, therefore, urgently needed to restore more natural biomechanics and improve long-term outcomes.

Customized root-analogue zirconia implants, designed via computer-aided design/computer-aided manufacturing (CAD/CAM) from cone-beam computed tomography (CBCT) images, can replicate natural tooth root geometry and provide a better fit with the alveolar bone. Their minimally invasive placement reduces tissue trauma, enhances initial stability, and shortens treatment time. Currently, these implants aim to achieve osseointegration similar to that of conventional implants.

Besides implant geometry, surface modification and 3D structuring have been explored to enhance cell adhesion and tissue regeneration [9]. Surface features, including topography and hydrophilicity and capillarity are essential for driving the angiogenic and osteogenic processes necessary for osseointegration. Regarding fiber restauration, various materials (e.g., HAp, PLA) and fabrication methods, such as electrospinning and melt electrowriting [10, 11], have been tested to optimize these properties. However, strategies are still needed to promote proper fibrointegration, particularly the perpendicular orientation of fibers characteristic of the natural PDL.

Advanced engineered 3D multistructure scaffolds with a gradient of micro-channels have been studied to induce peridontium complex tissues formation, namely cementum-dentin interface, PDL and bone [10, 12–16]. Abraham et al. [12] produced an angulated direction-oriented tunable 3D PLA-based scaffold to imitate the three layers (cementum, PDL, and alveolar bone). They observed that the scaffold provides guidance for the cell and can be customized to provide different oblique and perpendicular orientations and some specificities from patients. R. Staples and co-workers [11] corroborated the controlled 3D orientation of PDL, both perpendicular and oblique, using a biphasic fiber-guiding scaffold consisting of two integrated compartments: a PDL compartment-a parallel arrangement forming 100 μm spaced channels and a bone compartment-pore size gradient (ranging from 200 to 1200 μm). C.H. Lee et al. [14] developed an HA-doped PCL-based trilayer scaffold with gradient microchannels of 100, 600, and 300 μm for cementum-dentin interface, the PDL compartment, and the alveolar bone section, respectively, where regeneration of multiphasic tissue was observed. In addition, Ti implants with acid-etched, sandblasted, or calcium phosphate-coated surfaces, when combined with PDL-derived cells, have been shown to promote the formation of a cementum-like layer and a PDL with fibers oriented perpendicular to the surface in animal models [17]. In another study, cell sheet engineering using PDL cells seeded on Ti surfaces in canine models has resulted in periodontal-like connective tissue organization and cementum-like deposition [18]. Although surface modifications or even biomimetic scaffolds in different materials capable of regenerating the bone-PDL-cementum complex and guiding PDL fiber orientation have been reported, studies exploring microstructured zirconia surfaces to direct fibroblast organization or mimic cementum and/or dentinal tubules function remain scarce. This gap is particularly evident for ceramic implant surfaces, highlighting the need for ceramic-based fibrointegration strategies.

In this work, it is hypothesized that bioinspired porous channel-embedded zirconia surfaces can enhance the adhesion and guide the orientation of human periodontal ligament fibroblasts (hPLFs), resulting in improved cellular behavior compared to other zirconia surfaces. The primary objective of this study is to evaluate fibroblast adhesion, proliferation, and alignment on these surfaces, providing proof-of-concept evidence for promoting perpendicular fibrointegration in zirconia root-analogue implants.

2 | Materials and Methods

2.1 | Production of Zirconia Specimens

In this work, zirconia green compacts were produced by cold pressing technique using Yttria-stabilized Zirconia (TZ-3YB-E) commercial powder with a uniform dispersion of 3% mol Yttria (Tosoh Corporation, Japan), with high purity (99%) and theoretical bulk density of 1.19 g/cm^3 [19]. This commercial powder is formed by spherical agglomerates with an average size of 60 μm and contains small crystallites that are about 36 nm in diameter [20], as shown in Figure 1.

For that, the powder was introduced into a stainless-steel mold with an internal diameter of 10 mm and then a pressure of 200 MPa was applied for 30 s. After that, the pressure was released, and the green compact was removed. A schematic representation is shown in Figure 2a. Finally, some of the samples were pre-sintered at 1150°C for 1 h, with a heating and cooling rate of 8°C/min for channels production. The

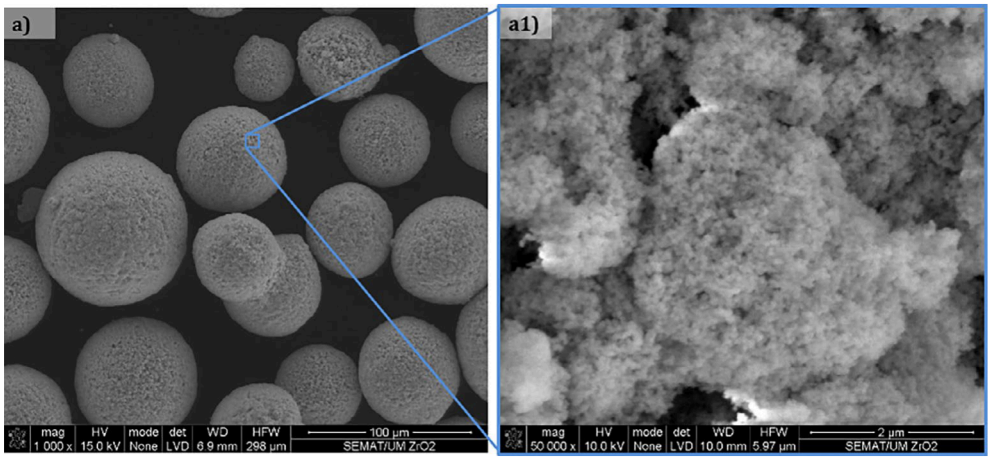

FIGURE 1 | SEM images of TZ-3YB-E commercial powder (Tosoh Corporation).

others were sintered at 1500°C for h, with a heating and cooling rate of 8°C/min to produce sandblasted surfaces for comparison purposes.

In the present work, four groups of zirconia samples were produced and further characterized, namely zirconia substrates dip-coated with a double layer of zirconia suspension (D), channeled zirconia surfaces (C), channeled zirconia and dip-coating (CD) and sandblasted (SB), which was tested as a control group, representing the surface that is commonly applied to the dental implants. After sintering, zirconia specimens were sandblasted with 180 µm spherical alumina particles for 20 s at a constant pressure of 6 bar at 7 mm, approximately, (between sample and blasting nozzle).

All samples were ultrasonically cleaned in isopropyl alcohol for 10 min to remove any loose debris or surface contamination.

2.2 | Channels-Embedded Porous Zirconia Surface Production

The channel dimensions, dip thickness, and porosity of the CD samples were selected based on literature data. Regarding porosity, dentin in natural tooth roots exhibits a porosity of 1% to 32%, facilitating fluid movement essential for nutrient delivery and waste exchange in the pulp-dentin complex, whereas cementum also exhibits a porous matrix, although its exact porosity and pore size remain poorly characterized [22–24]. Additionally, acellular cementum thickness has been reported to range from 50 to 200 µm depending on age [25].

Channel dimensions were defined considering the average width of the PDL (approximately 150–380 µm) [26] and the optimal pore size for fibroblast growth reported by A. Zaeri et al. [27] (290 to 310 µm). These findings, together with developed previous work [21], guided the design of the samples, including channel diameter, porosity (approximately 9%), and thickness (167.04 ± 51.87 µm) to replicate the functional and morphological features of natural dentin and cementum, while supporting fibroblast attachment and PDL-like tissue formation and preserving the mechanical constraints of the zirconia substrates. Channels were initially drilled with a 400 µm tool. Following sintering, the material underwent shrinkage, yielding a final channel diameter of approximately 322 µm, which aligns closely with reported values in the literature. This size provides sufficient space for fibroblast alignment and extracellular matrix deposition.

2.2.1 | Channels Structure Manufacturing

To replicate the capillarity and vascularization of natural dentinal tubules within the zirconia root-analogue implant, channels with diameter (ø) of 400 µm and interspace (d) of 300 µm were produced in pre-sintered zirconia green compacts by CAD/CAM technology in a *Roland DWX 50* CNC milling machine, as shown in Figure 2b.

2.2.2 | Porous Zirconia Surface Production

In natural teeth, PDL fibers are anchored by the cementum surface, which is considered a key structure by some researchers. Although there is no consensus, some studies [22–24] have shown that cementum morphology has a porous matrix. However, its specific porosity and pore diameter are still poorly understood. In this work, a porous surface was produced aiming to mimic cementum function, namely, to anchor PDL fibers onto the implant surface.

The production of porous zirconia surface was conducted by dip coating process following the procedure used by S. Roedel et al. [20]. For that, the commercial zirconia powder TZ-3YSB-E, *TOSOH* was used in two different forms, as schematically represented in Figure 2c:

i. *Fine powder*—prepared by sonicating the commercial powder (30 vol% of solid content in an ultrapure water suspension) using a Hielscher UP200St ultrasonic probe for 1 min to break up agglomerates, resulting in particle sizes ranging from approximately 3 to 10 µm [20]. The green fine powder did not undergo heat treatment.

ii. *Coarse powder*—produced through pre-sintering of the commercial powder at 1150°C for 1 h with a heating rate

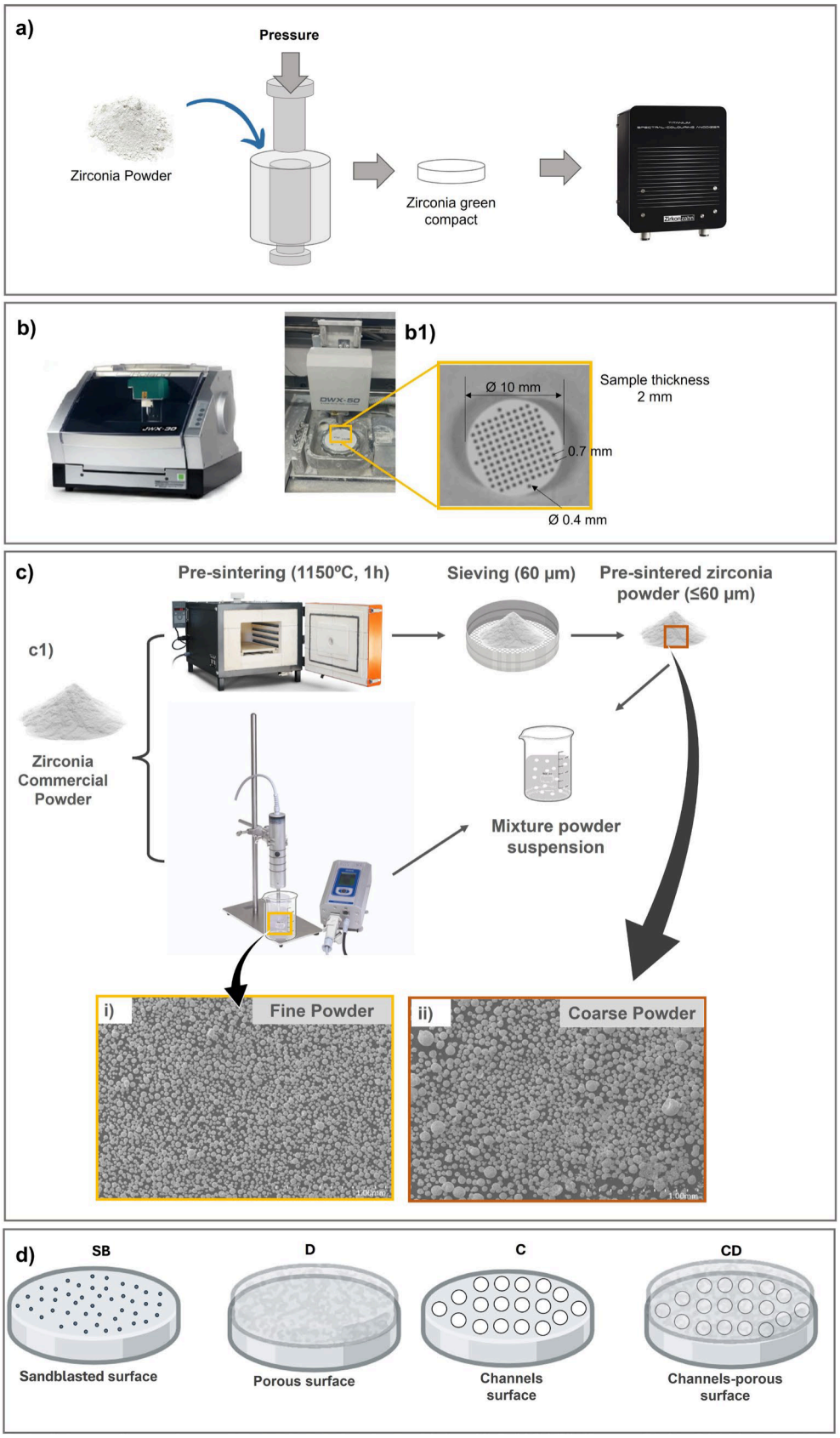

FIGURE 2 | Schematic representation of zirconia specimens' production. (a) zirconia green compacts production; (b) zirconia channels structure manufacturing by CNC milling. *Roland DWX 50* CNC milling machine; (b1) Machining system and the final channeled zirconia specimens at green state; (c) zirconia powders preparation: (i) fine powder and (ii) coarse powder; and (d) all produced zirconia specimens. Figures adapted from Proença et al. [21].

of 5°C/min to consolidate the granules. Then, the material was sieved through a 60 μm mesh to obtain a narrower particle size distribution, resulting in an average particle size of 34.44 ± 14.66 μm.

For dip coating, two suspensions were prepared: (i) a fine powder suspension—prepared with 30 vol.% of the green solid content and (ii) a mixture (finer and coarse) powder suspension—prepared with 25% vol. of fine powder and 75% vol. of the coarse powder and 2 wt.% of the dispersant agent carboxmymethylcellulose (CMC) from Sigma-Aldrich. Dip coating was performed in custom-made equipment, using a fixed speed of 4 mm/s and an immersion time of 5 s. Initially, specimens (green state) were immersed into a fine powder suspension to create an initial thin adhesive layer followed by air drying for 20 min. Afterwards, specimens were immersed in the powder mixture suspension followed by air drying for 20 min. The last process was repeated since the porous surface is completed after 2 immersions in the powder mixture suspension. Finally, specimens were sintered in a conventional *Zirkonzahn* furnace at 1500°C for 2 h. It should be noted that in case of samples containing channels, one side of the specimen was coated with wax to fill the microchannels, preventing it from being covered by the porous zirconia coating. During the sintering process, the wax was sublimed.

Thus, and as represented in Figure 2d, four different types of specimens were produced: (1) specimens subjected to sandblasted (SB); (2) specimens with channels (C); (3) specimens with dip coating (D); and (4) specimens with channels and dip coating (CD).

2.3 | Cell Culture

hPLF (HPDLF, 2630, ScienCell Research Laboratories, CA, USA) are isolated from human periodontal tissue and display distinct functional activities in the maintenance of the integrity of this tissue. The cells were routinely grown in Dulbecco's modified Eagle's medium (DMEM) with phenol red, supplemented with 15% (v/v) Fetal Bovine Serum (FBS), 1% (v/v) L-glutamine, and 1% (v/v) Penicillin/Streptomycin, in a humidified incubator with a 5% CO_2 atmosphere and at 37°C. The medium was changed every 2 days until the culture reached the right confluence. The cells were allowed to proliferate until they reached 95% confluence, treated with 0.25% trypsin, and were subcultured in 75 cm^2 flasks once a week.

2.4 | Cell Viability Assay

To evaluate hPLFs adhesion and migration through the porous structure and channels, the specimens were placed in a 24-well plate. Silicone was used to encase the specimens, creating a barrier between two media with different FBS concentrations, as shown in Figure 6. For that, a 3D mold was designed and produced.

Underneath each specimen, complete medium with 10% FBS was used. On top of each specimen, a drop of 30 μL containing 1.5×0^4 cells was placed. After 30 min, each well containing the zirconia discs was filled with medium containing 2% FBS, to submit the cells to serum deprivation, thereby stimulating them to migrate toward a better nutrient supply. The medium exchange can only occur through the zirconia specimens, as they were sealed with silicone. Life and death control (30% DMSO) was performed. After 3 and 7 days, 3-(4,5-dimethylthiazol-2-yl)-5-(3-carboxymethoxyphenyl)-2-(4-sulfophenyl)-2H-tetrazolium (MTS) cell proliferation colorimetric assay kit (Biovision, USA) was used to evaluate the viability of cells through their metabolic activity in the mitochondria. The medium was removed, and MTS was added to each well. The cells were incubated for 3 h at 37°C in a humidified incubator with 5% CO_2. Afterwards, 150 μL was transferred to a well of a 96-well plate and the absorbance was read at 490 nm using a microplate reader (Epoch, BioTek, Santa Clara, CA, USA). The absorbance values obtained were normalized to the 10% FBS control group to account for baseline differences in cell metabolic activity. This normalization ensures that comparisons between surface groups reflect relative changes due to surface architecture rather than variations in baseline viability.

2.5 | Surface and Morphological Characterization

The two zirconia powders (fine and coarse), as well as the surface of all zirconia specimens, were analyzed using Field Emission Gun Scanning Electron Microscopy (FEG-SEM) with a Hitachi FlexSEM1000II scanning electron microscope (Tokyo, Japan). SEM images were collected using both backscattered (BSE) and secondary electron (SE) detectors, with an accelerating voltage ranging from 10 to 15 kV and a spot size between 30 and 40. Prior to analysis, the samples were coated with gold for 60 s using a Quorum Mini-QS (England) sputter coater.

SEM was also used in the in vitro tests to assess the ability of hPLFs to adhere and spread as well as to determine cell morphology after 3 and 7 days of culture. After washing with sterile PBS, all specimens containing cells were fixed with a 2.5% glutaraldehyde (Sigma, USA) solution in PBS. The specimens were then dehydrated in increased concentrations of ethanol from 30% to 100% and air-dried overnight. Before being observed in SEM, the specimens were coated with gold. For cross-section analysis, the samples were manually fractured by applying mechanical force.

Surface roughness of CD samples was measured using a contact profilometer (Surftest SJ-201, Mitutoyo, Tokyo, Japan). For each specimen, four linear scans were acquired over a length of 5 mm at a scanning speed of 0.5 mm/s using a diamond stylus (2 μm tip diameter). The average surface roughness (Ra) was evaluated, as described by Proença et al. [21].

2.6 | Electrical Impedance Measurement on Biological Systems (Specimens-Fibroblasts)

Cell-based impedance (CBI) is a non-destructive and sensitive technique that uses the principles of electrochemical impedance spectroscopy (EIS) by measuring changes in electrical impedance relative to a voltage applied to a cell layer. It has been employed to monitor cell proliferation, metabolism, and

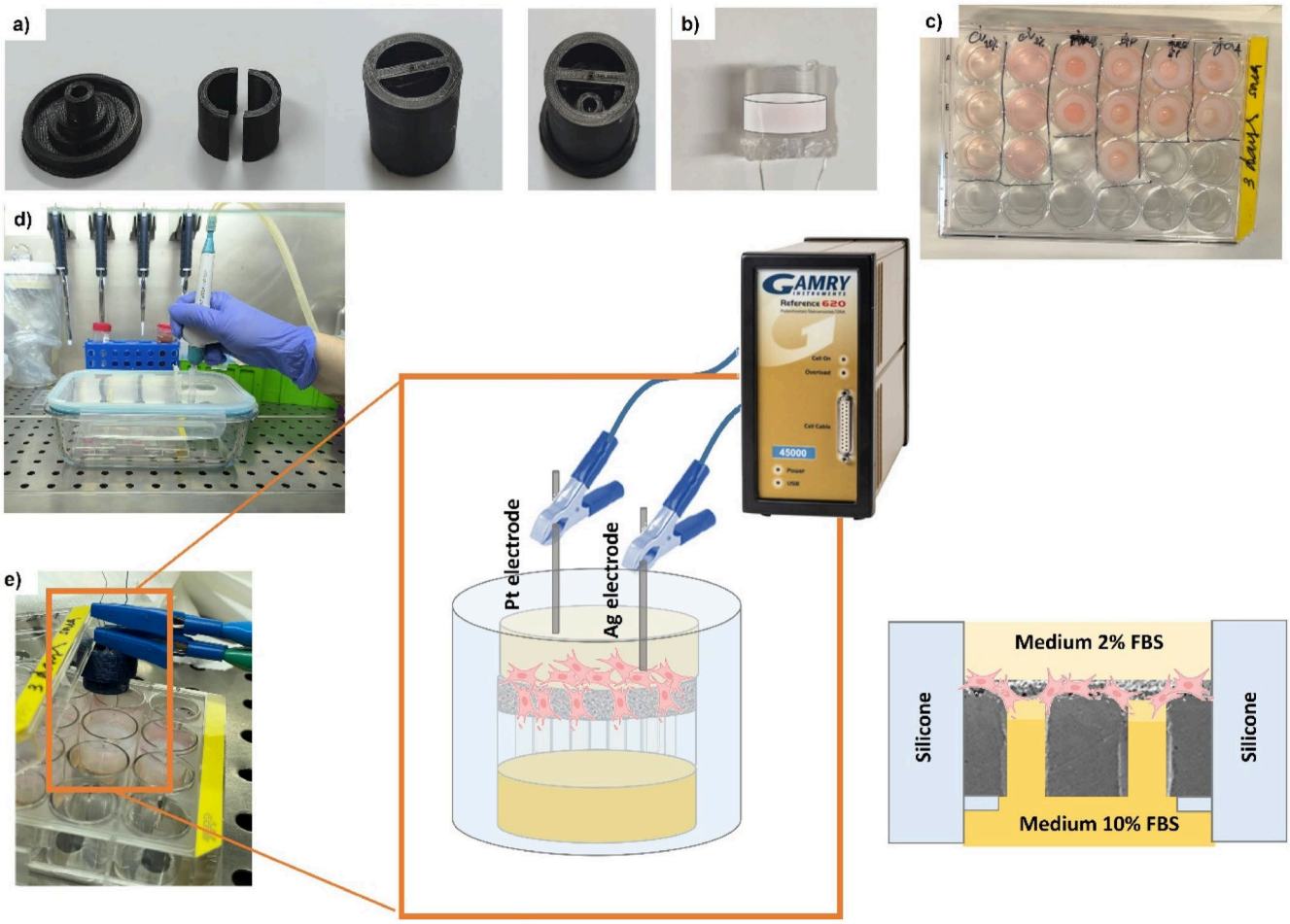

FIGURE 3 | hPLFs in vitro test with different percentages (%) of FBS. (a) 3D PLA mold for silicone used for silicone preparation, (b) sample supported by silicone to introduce in 24 well plate, (c) 24 cell plate with samples supported by silicone and embedded in medium, (d) Vacuum system to remove bubbles inside of channels, and (e) schematic representation of electrical cell impedance measurement.

viability in real time [28–31], in both 2D and 3D cell culture, as well as to study the electrochemical and corrosion behavior of metal implant surfaces under the simulated inflammatory conditions [32, 33]. More than that, this method can provide smart monitoring of cellular conditions and responses to extracellular stimuli in the biomedical field [34].

In this work, the electrochemical impedance measurements were carried out to evaluate the behavior of fibroblasts cultured on zirconia substrates. In general, studies [29, 30] typically employ EIS systems with planar electrode geometries, where cells are cultured directly on conductive surfaces. However, in this study, the substrates were made of zirconia, a non-conductive material, which required an alternative approach to the standard setup. Thus, the measurements were performed by means of GAMRY 600+ equipment using a two-electrode configuration, with one electrode (silver (Ag) wire with 0.3 mm of diameter) placed in direct contact with the adherent cell layer and the other (platinum (Pt) wire with diameter of 0.406 mm) positioned in the culture medium. Impedance magnitude (|Z|) was recorded across a frequency range from 1 to 100 kHz, with a 10 mV of amplitude, with 10 points per decade. The experiments were conducted at 37°C, which mimics the human body temperature and provides physiologically relevant conditions for the fibroblasts. This setup allowed indirect assessment of cell–substrate interactions and cellular behavior on zirconia surfaces. The measurements were performed on specimens after 3 and 7 days of culture in a 24-well plate, as shown in Figure 3.

2.7 | Statistical Analyses

Statistical analyses were conducted using GraphPad Prism version 9.4.1 (GraphPad Software, San Diego, CA, USA.). All assays were performed with at least in duplicate, and each experiment was independently repeated at three times ($n = 3$ per group). Data normality was assessed with Shapiro–Wilk's test. Given the limited number of biological replicates and the absence of normal data distribution, non-parametric statistical methods were applied.

The comparisons were defined a based on the study hypothesis and included: (i) sandblasted (SB) zirconia (control) versus porous (D) and channeled (C) zirconia surfaces, and (ii) porous (D) and channeled (C) zirconia surfaces versus channel-embedded (CD) configurations. These comparisons were designed to evaluate the effect of surface porosity and the additional impact of embedded channels on fibroblast adhesion, proliferation and

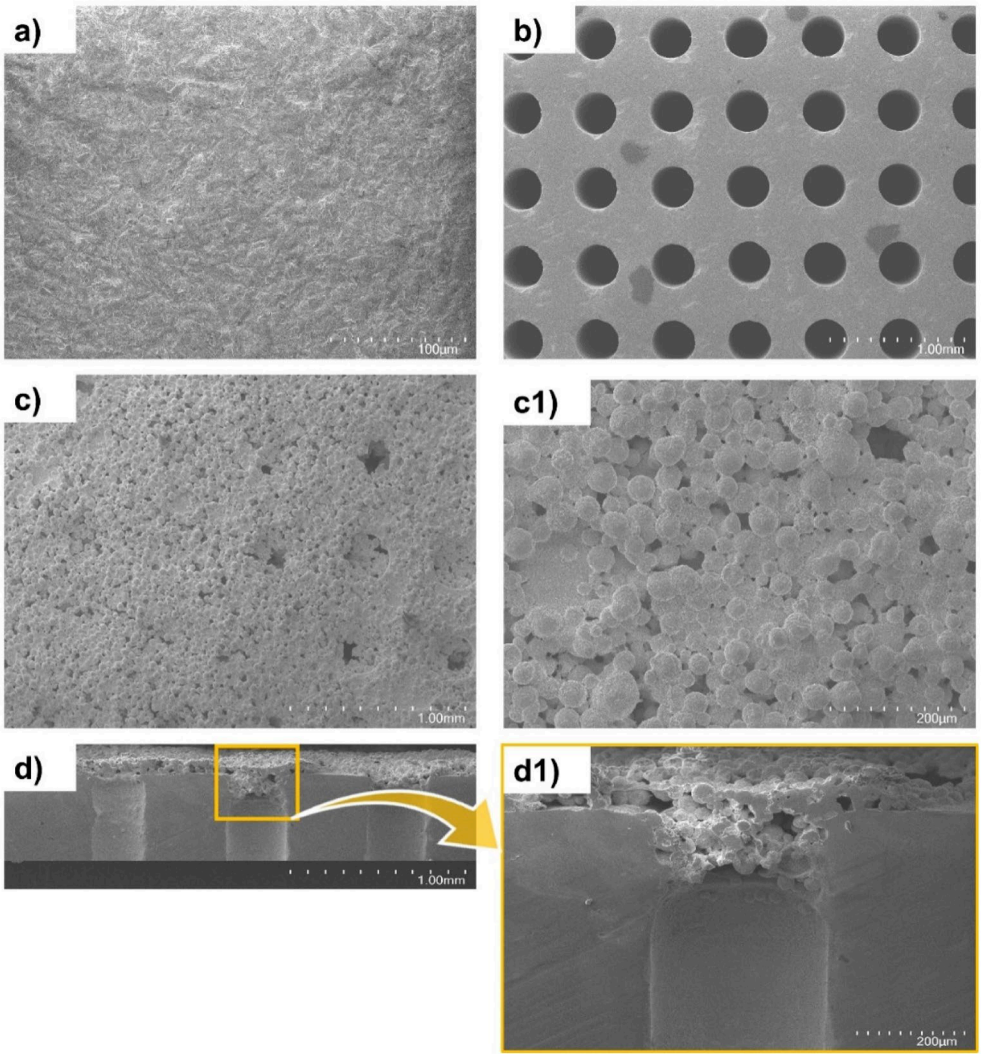

FIGURE 4 | Top-view SEM images of the (a) SB, (b) C, and (c-c1) D specimens and cross-section of CD specimen (d-d1). Figures adapted from Proença et al. [21].

alignment. Analyses were performed using the Kruskall-Wallis's test, followed by Dunn's post hoc test. Results are presented as mean ± standard deviation. Exact p values are reported for all comparisons, and effect sizes where calculated where applicable. Results were normalized to the 10% FBS control to account baseline differences in cell behavior. Statistical significance was considered at $p < 0.05$ (*$p < 0.05$; **$p < 0.01$; ***$p < 0.001$; ****$p < 0.0001$).

3 | Results and Discussion

3.1 | Specimens' Characterization

The implant integration is directly influenced by its surface roughness, which affects cell proliferation and differentiation, extracellular matrix synthesis, local production factors, and even cell morphology.

Furthermore, a surface with microporosity is crucial to occur angiogenesis, nutrient diffusion, the removal of metabolic substances and the migration, distribution and proliferation of cells, to lead to tissue formation [35]. If the pores are too small (around 50 µm), the cells are unable to migrate toward the center, resulting in the formation of a cellular capsule around the edges. Conversely, pores that are too large to support orientation but to reduce contact surface area, limiting cell adhesion [36].

The four produced surfaces were inspected by SEM, and the top and cross-section views are presented in Figure 4.

In Figure 4a which corresponds to the SB surface, commonly used in commercial implants, it is possible to observe an irregular surface with a surface roughness of 1.17 ± 0.21 µm [21]. Figure 4b corresponds to zirconia with micro-channels with an average diameter of 322 ± 7.86 µm produced by a CNC milling system to mimic dental tubule's function, more specifically, to induce perpendicular fibroblasts growth and thus, to attain fibrointegration. According to the A. Zaeri et al. [27], for vascularization and angiogenesis, the ideal pore size ranges from 160 to 270 µm, while interconnected pores of 300–500 µm enhance nutrient exchange. Regarding cell growth, chondrocytes and osteoblasts thrive in pores of 380–405 µm, whereas fibroblasts and bone formation are favored in pores of 290–310 µm. For

proliferation and migration, optimal pore sizes are approximately 100 μm for osteoblasts, greater than 300 μm for fibroblasts, and 250–500 μm for chondrocytes. J.H. Nam and co-workers [37] observed more robust growth of chondrocytes and fibroblasts in scaffolds with pore sizes of 300–400 μm after several weeks of culture. In another study, F. Mukasheva et al. [38] reports that pore sizes above 200 μm favor fibroblast migration and proliferation. Additionally, A. Zaeri et al. [27] reports that the optimal pore size for fibroblast growth ranges from 290 to 310 μm, which is close to the micro-channels' size obtained in this study. Figure 4c–c1 show top view images of the porous structure produced by dip coating of zirconia suspensions. This outermost layer will be important to promote a strong adhesion and spread of fibroblasts on the root-analogue implant surface, like the role of the cementum structure promote at the natural tooth. This layer presents an average thickness of 167.04 ± 51.87 μm and a relative porosity of 9% [21]. Low porosity in zirconia preserves mechanical stability and dimensional fidelity, which are critical for maintaining space, load transfer, and interface integrity in periodontal environments [39, 40]. The structure presents interconnected pores that cover the entire surface and even extend into the interior of the channels, establishing communication with internal micro-channels and promoting strong adhesion to the zirconia substrate, as shown in Figure 4d–d1. Besides that, some micro-channels remain open. A previous study conducted by Proença M. and co-workers [21] demonstrated that this porous structure shows strong adhesion to the zirconia substrate with channels and exhibits high wettability displaying superhydrophilic behavior (contact angle ≈0°).

These characteristics are advantageous for enhancing the stability of the coating and promoting better interaction with fluids and fibroblasts' attachment, thereby improving the surface performance.

3.2 | In Vitro Human Periodontal Fibroblasts Viability

Compared to other tissues in the body, the PDL has a relatively limited regenerative capacity. In cases of tooth abnormalities, especially when they involve extensive damage, disease, or even tooth extraction, the regenerative potential of the PDL may be compromised or even absent. PDLFs are spindle-shaped, elongated connective cells that constitute approximately 50%–60% of the total periodontal cell population. Their multidirectional differentiation potential allows them to contribute to tissue restoration and regeneration following injury. They play a critical role in the repair, maintenance, and regeneration of the PDL, specifically in the synthesis and remodeling of the extracellular matrix, particularly by secreting collagen types I and III. They also contribute to the maintenance of the periodontal space by balancing both collagen synthesis and degradation, facilitating cell communication with osteoblasts, cementoblasts, and immune system cells, and responding to mechanical stimuli such as masticatory and orthodontic forces [41, 42].

In response to stimuli, these cells can migrate and align in specific orientations: in a discrete linear manner, parallel to collagen fiber bundles, forming an extensive cellular network between the cementum and alveolar bone. They are capable of secreting collagen and elastin, organizing them into fibers to form the extracellular matrix [42], both in oblique and perpendicular directions. Furthermore, the modulation of signaling pathways and the smart induction of oriented fibroblast growth represent not only a challenge but also a promising idea, in the context of the PDL, aiming to guide fibroblasts to their proper location and function.

Chemotaxis is described as the directional migration of cells toward a concentration gradient of chemoattractants [43]. Fetal bovine serum (FBS) is the most used supplement for cell cultures due to its high levels of growth-stimulating factors [44–48]. It can influence cell proliferation and differentiation, modulation of molecules and cellular mechanisms, cell viability, and cytokine production [49]. Therefore, it was used here as a promising initial candidate to establish a chemoattractant gradient for a chemotaxis assay. The hPLFs were exposed to a gradient of 2% and 10% FBS-containing medium between each of the four tested zirconia samples. The cells were in contact with medium containing only 2% FBS on the top surface of each zirconia specimen, while 10% FBS medium (the most commonly used concentration) was placed at the bottom of the well, creating a concentration gradient. Each specimen was surrounded by a silicone support to ensure that medium flow and exchanges occurred exclusively through each sample.

The cellular viability of hPLFs at 3 and 7 days was assessed using the MTS assay, and the results are shown in Figure 5a. Figure 5b presents microscope images of control hPLFs cultured with 2% and 10% FBS at the time of seeding and after 3 days. When comparing the control cell groups (cells cultured with 2% and 10% FBS), the results suggest higher viability for cells cultured in medium supplemented with 10% FBS, although statistical significance was not reached. This result is in line with findings reported in the literature [45, 47, 50] which have shown higher cell viability for higher FBS concentrations in the medium up to 10%. The concentration of FBS is related to the availability of nutrients, growth factors and essential proteins for cell survival and proliferation. This means that at lower concentrations, the lack of these factors can affect viability, proliferation, and morphology, as well as induce cellular stress. Therefore, although the FBS gradient model provides a controlled chemotactic stimulus, it represents a simplified in vitro system. Serum deprivation may influence fibroblast behavior independently of surface architecture, and the observed cellular distribution may reflect a combination of directional migration, selective adhesion, and survival effects rather than purely chemotactic guidance.

The results are consistent with the images shown in Figure 5b. After 3 days of cell culture, several aspects were observed in hPLFs cultured with 2% FBS: a decrease in cell proliferation, indicated by the reduced number of cells; a spherical shape of the fibroblasts, suggesting morphological alterations due to the lack of support for maintaining their normal structure; and increased turbidity in the culture medium, likely caused by cellular stress. Under stress, certain cellular defense mechanisms may be triggered, such as the release of cytokines, which can affect cell function and potentially lead to apoptosis [51–53].

The results of cell viability revealed that all these zirconia specimens are biocompatible with hPLFs (all cell viability values are

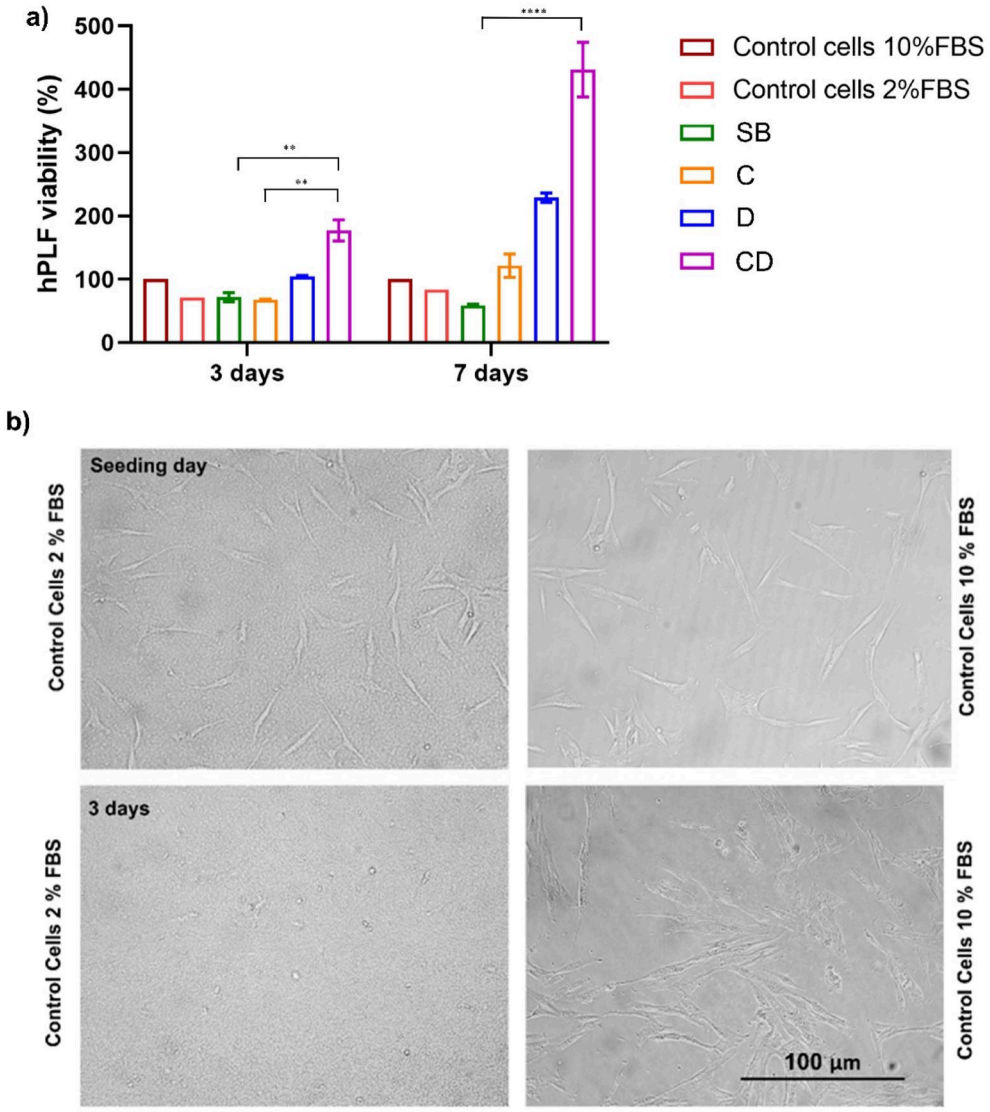

FIGURE 5 | (a) Cell viability of hPLFs in direct contact with SB, C, D and CD zirconia surfaces, presented as mean ± SD ($n = 3$ per group). The results were normalized to the 10% FBS control group to account for baseline differenced in cell behavior. Statistical comparisons were performed using the Kruskall-Wallis test with Dunn's post hoc test; exact p values are indicated as $^{*}p < 0.05$; $^{**}p < 0.01$; $^{***}p < 0.001$. (b) Representative microscope images of control cells cultured in 2% FBS and 10% FBS at the time of seeding and after 3 days.

above 70%). It is known that zirconia has no cytotoxic effects on several types of cells, being biocompatible, supporting cell survival and proliferation [54, 55]. After 3 days, the highest hPLFs viability percentage was achieved by CD zirconia surfaces, followed by the D surfaces, and C and SB surfaces. A statistically significant difference in cellular viability on zirconia surfaces is clearly observed on CD zirconia surfaces compared to C and SB zirconia surfaces ($p < 0.01$). The same tendency was observed after 7 days of cell culture.

Figure 6 presents SEM images of PDL fibroblasts attached to all tested surfaces, taken after 3 and 7 days of culture. Sandblasting is the conventional surface treatment employed in dental implant surfaces characterized by increased surface roughness aimed to improve osseointegration. In fact, several studies [56–59] have reported high cell adhesion and proliferation results when compared to those without any treatment. In this study, cells are homogeneously distributed across the SB surface and adhere within the cavities resulting from the blasting process (Figure 6a,b), but do not produce protrusions to communicate with each other. This is observed at both time points. In the case of micro-channels, although this structure allows access to more nutrients and growth factors from the medium with a higher concentration of FBS coming from the bottom, the absence of any rough or porous structure at the top of the sample results in a lack of contact points for the fibroblasts to adhere, communicate, and proliferate. As a result, the cells detach during the fixation and dehydration process and cannot be visualized in the SEM images, as shown in Figure 6c. This occurs at both 3 and 7 days after culture. Moreover, the obtained results showed that better outcomes can be achieved through the development of engineered solutions/strategies capable of smartly inducing cell growth, spreading and orientation.

As can be seen in Figure 6d, the porous structure exhibits a rougher surface with high porosity and well-interconnected

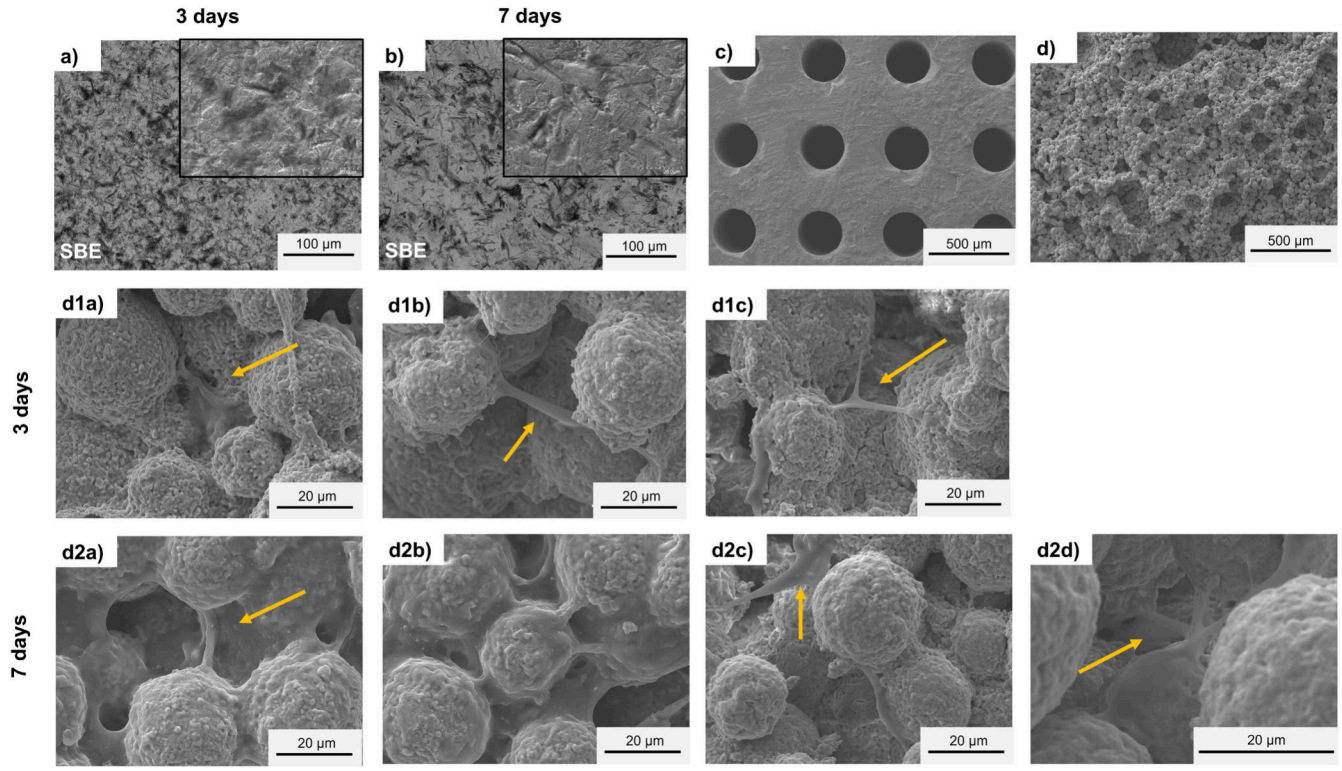

FIGURE 6 | SEM micrographs of zirconia surfaces of hPLFs of SB surface: (a) 3 days and (b) 7 days; (c) C-channeled surface and (d) D surface: (d1a–d1c) 3 days and (d2a–d2d) 7 days.

pores. According to the literature [60], these features promote cell adhesion, facilitate cell-cell communication as well as gas and nutrient exchange for cell proliferation. In these surfaces cells are not visible as they migrate into the porous structure as evidenced by Figure 6d1a. After 3 days of culture, fibroblasts begin to change their morphology and form connections between different points as observed in Figure 6d1b,d1c (highlighted by orange arrows). Over the course of the culture period (7 days), the cells continue their activity, increasing the number of connections and covering the porous structure as shown in Figure 6d2a–d2d. These findings indicate that D surface is highly suitable for fibroblast adhesion and proliferation.

Regarding CD surfaces (Figure 7), the fibroblasts are well adhered to the porous structure covering the entire surface and have spread effectively throughout the interconnected pores, including deep within the porous layer and reaching the entrance of the microchannels which have a diameter of 300 µm, visible through cross section views shown in Figure 7a–a4. This indicates that the fibroblasts migrate from the top of the surface (across the porous layer) toward the microchannels, where they encounter a higher availability of nutrients and growth factors from the FBS-enriched (10%) medium present within the channels. Moreover, the hPLFs appear to communicate with each other, establishing visible connections through their extensions (indicated through yellow arrows), with a spindle-like shape, called filopodia. Filopodia which are actin rich structures, are found in many different cell types, such as fibroblasts and neurons [61]. Filopodia are important for cell migration during wound healing [62]. This physiological structure can exhibit different morphologies and often displays protrusive, retractile, and sweeping motility, but can also exist as stationary, anchored cellular extensions. Because of their elongated geometry, filopodia can reach, detect, and grasp distant targets [41]. Accordingly, filopodia are believed to guide cell locomotion during normal tissue morphogenesis by recognizing adhesive surfaces and making initial contacts with the extracellular matrix [41]. The same behavior is observed at surfaces after 7 days. However, due to the higher cell density, it is less clearly visible.

Thus, the results suggest that CD zirconia surfaces combining internal micro-channels and external porous structures enhance fibroblast attachment and spreading compared to the other tested configurations. These findings support their potential application in zirconia root-analogue implants as a strategy to promote structured fibre alignment. Furthermore, the possibility of customizing channel orientation through CAD/CAM fabrication may allow modulation of both perpendicular and oblique cellular growth patterns. However, further biological and functional validation is required to confirm effective fibrointegration.

3.3 | Electrical Impedance Evaluation

The literature reports that the impedance of cells has been measured in different ways: in single cells, multiple cells, cells in suspensions or cells adhered to substrates, either through single-point measurements or continuous long-term monitoring [29]. In this work, electrical impedance was used to assess fibroblast behavior on different zirconia surfaces, with the significance of the results supported by comparative analysis across the tested conditions. Particular focus was given to channel-embedded porous zirconia surfaces, designed for application in zirconia

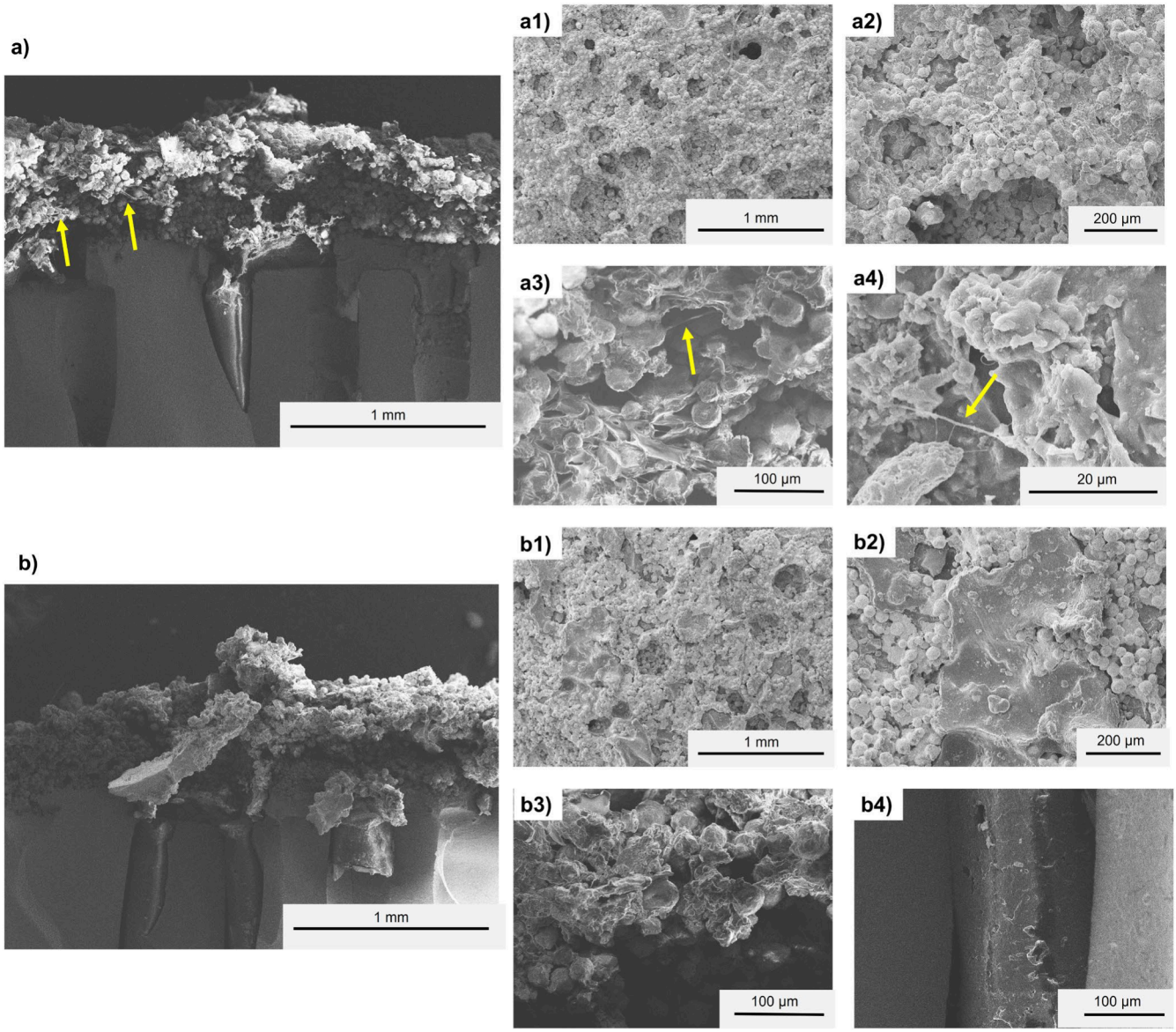

FIGURE 7 | SEM micrographs of CD zirconia surface of hPLFs of (a) after 3 days of culture and (b) after 7 days.

root-analogue implants to promote fibrointegration. Although zirconia is non-conductive and the measurements were not performed directly at the cell membrane using specific nano- or micro-probes, changes in impedance reflect complex contributions from the medium, electrode interfaces, and cell layers, and may provide indirect information about key cellular processes such as adhesion, spreading, proliferation, and confluence. The setup consisted of one electrode in contact with the adherent cell layer and another electrode positioned in the culture medium, as schematically represented in Figure 3 in the materials and methods section.

Figure 8 presents the impedance results represented as Bode plots for each tested zirconia surface, measured after 3 and 7 days of culture, across a frequency range from 1 to 100 kHz. The impedance of both FBS-enriched (10%) and FBS-poor (2%) media without cells was also separately measured as a control. Since there were no cells present, there was no cellular layer formed, and thus, the electrodes were in direct contact with the culture medium rather than a cell layer. It should be noted that the measured impedance magnitude reflects contributions from both the medium or cell layer and the electrode-electrolyte interface, which may be influenced by the applied 0.4 V potential between the Ag and Pt electrodes. For simplicity and clarity, the impedance results are reported as magnitude of impedance (|Z|). While the real (Z′) and imaginary (Z″) components provide additional insights into resistance and capacitance contributions, the magnitude sufficiently reflects the integrity and confluence of the cell layer for comparative purposes.

The impedance magnitude decreased with increasing frequency for all conditions, consistent with the capacitive behavior of cell membranes and adherent cell layers reported in the literature [29, 63–65]. This behavior was observed across all conditions, including the fibroblast control, at both 3 and 7 days of culture, indicating that it is independent of both culture duration and cell-substrate interaction type.

After seeding, cells begin to adhere, migrate, and modify their morphology while interacting with both the substrate and

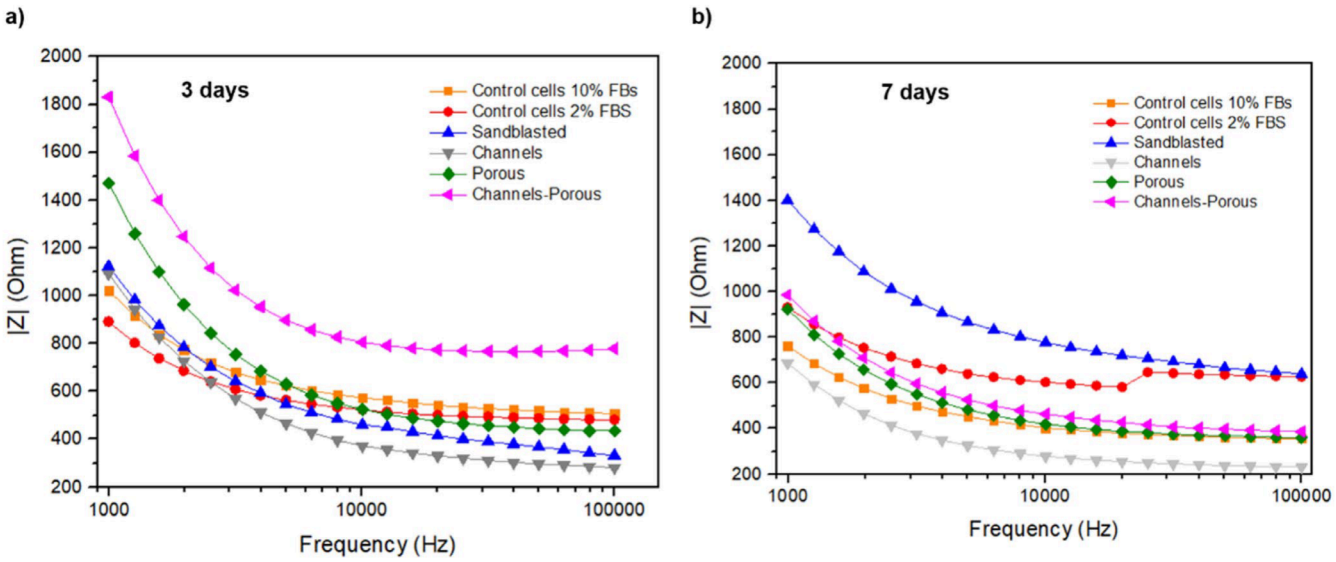

FIGURE 8 | Magnitude of Impedance |Z| (Ohm) as a function of frequency for different zirconia tested surfaces.

neighboring cells. They actively sense and respond to changes in the topographical, physical, and chemical properties of their environment [34].

At Day 3, quantitative comparison across groups revealed that CD zirconia specimens exhibited the highest impedance values over the entire frequency range, followed by D specimens, while C, SB, and control conditions showed significantly lower impedance. The increased impedance of CD surfaces can result from a combination of enhanced cell adhesion and spreading, increased cell density, and modifications of the electrode-cell-medium interface, where the organized cell layers partially impede current flow while changes in medium conductivity due to metabolic activity further modulate the signal. The larger effective surface area and microtopographical features of the porous layer, combined with the presence of channels that facilitate nutrient and oxygen diffusion from the nutrient-rich medium, support the formation of a more cohesive and electrically resistive cell layer. The D specimens also showed elevated impedance, particularly at low frequencies (< 10 kHz), highlighting the dominant role of the porous coating in promoting fibroblast adhesion and proliferation. In contrast, specimens containing only channels exhibited lower impedance values, indicating that channels alone are insufficient to sustain a dense adherent cell layer at the measurement interface.

After 7 days of culture, a shift in impedance behavior was observed, with higher impedance values on SB surfaces compared to D and CD specimens. This result cannot be solely attributed to cell number or viability and likely reflects a combination of factors. Dense cell layers forming on the sandblasted surfaces, extracellular matrix deposition, and improved contact between cells and the electrode due to surface micro-roughness may all contribute to increased impedance. In contrast, the lower impedance measured on D and CD surfaces at this time point is consistent with a more spatially distributed, three-dimensional cell organization, involving cell migration and proliferation within the porous coating and channels partially reducing their direct contribution to the electrode interface. This interpretation is supported by the hPDLF viability data (Figure 5) and cross-sectional SEM observations (Figure 7), which indicate reduced cell density at the electrode–electrolyte interface despite sustained cellular activity. Variations in medium conductivity and local capacitive effects may further modulate the signal, highlighting the complex interplay between surface topography, cell morphology, and measurement conditions.

Across all surfaces, impedance decreased from day 3 to day 7. This temporal reduction likely results from changes in cell morphology, redistribution within the substrate architecture, and increased medium conductivity due to metabolic byproducts, rather than a loss of viability. Similar trends have been reported for fibroblasts and stem cells during prolonged culture after peak spreading or confluence. As cultures mature, cells may undergo reorganization, reduced adhesion, or partial detachment, leading to a less cohesive barrier at the measurement interface [34]. A. Kociubiński [66] reported in their study that measured impedance values change with the reactivity of the cells in contact with a material. They observed that in adherent mouse fibroblasts, impedance initially increases during spreading and proliferation phases but then decreases when apoptosis or overgrowth occurs. In another study, R.C. Nordberg and coworkers [67] reported a decrease in impedance after reaching peak confluence of human adipose stem cells, even though cell viability was maintained.

Interestingly, control fibroblasts cultured in 2% FBS exhibited higher impedance over time compared to those in 10% FBS. This may be attributed to the slower proliferation rate corroborated by the hPLFs viability results depicted in Figure 8. However, over time, increased secretion of ionic byproducts, higher medium conductivity, and potential disruption or remodeling of the cell layer contribute to a reduction in impedance. R. Ramos et al. [68] studied the electrical properties of cell-mediated mineral deposition process for 28 days and they reported that during prolonged periods of cell culture the impedance tends to decrease over time, because of the metabolic byproducts or mineral deposition.

Finally, these results indicate that substrate architecture may influence the spatial distribution and attachment of fibroblasts, which could indirectly affect nutrient accessibility, but direct mechanistic conclusions cannot be drawn from impedance data alone.

Additional modifications and improvements can be made to tailor this strategy along the implant, providing specific characteristics for PDL fibroblasts on the root-analogous portion, as well as for gingival fibroblasts on the coronal part, thereby also contributing to the protection of the peri-implant zone against bacterial invasion. However, regarding translational future studies, such as in vivo validation, mechanical testing under cyclic loading, and bacterial adhesion assays, will be essential to evaluate the clinical feasibility and functional performance of these surfaces.

4 | Conclusions

This study investigated the potential of bioinspired zirconia surfaces to enhance fibroblast adhesion and support guided cellular orientation, representing an initial proof-of-concept toward structured fibrointegration inspired by the natural tooth interface. Zirconia surfaces featuring channels and porous structures mimicking dentinal tubules and cementum functions, respectively, were successfully produced by CAD/CAM and a two-layer zirconia dip-coating process. The response of hPLFs to the developed surface was evaluated through in vitro tests supported by electrical impedance measurements, from which the following key conclusions can be drawn.

- The channel-embedded porous zirconia surfaces exhibited the highest hPLF cell viability after 3 and 7 days of culture compared to porous, channel, and conventional sandblasted surfaces.
- After 3 days of culture the channel-embedded porous zirconia surfaces exhibited the highest magnitude of cell layer impedance among all tested surfaces. This result showed that porous coating plays an important role on cell adhesion, proliferation and migration into 3D structure, while the channels enhance this effect through nutrients and oxygen support from FBS-enriched medium.

In conclusion, channel-embedded porous zirconia surfaces demonstrated enhanced fibroblast adhesion and spreading in vitro, supporting their potential as a strategy to guide structured cell organization. This bioinspired design represents an initial proof-of-concept toward improving soft tissue interaction at the implant interface. While the favorable response of human PDL fibroblasts and the feasibility of CAD/CAM fabrication of root-analogue zirconia implants are encouraging, these findings remain preliminary. Further mechanical evaluation under static and dynamic loading conditions, as well as advanced biological studies using 3D models and in vivo systems, are necessary to determine long-term stability, functional integration, and true translational relevance under physiological conditions.

Author Contributions

Joana Ribeiro: Writing – original draft, investigation and formal analysis. Manuela Ribeiro: investigation and formal analysis. Flávio Rodrigues: investigation and formal analysis. Diego Chaves: formal analysis. Diana P. Ferreira: formal analysis. Lia Rimondini: Writing – review and editing and conceptualization. Michael Gasik: writing – review and editing and conceptualization. Filipe S. Silva: writing – review and editing, supervision, resources, project administration, funding acquisition and conceptualization. Sara Madeira: writing – review and editing, supervision, resources, project administration, investigation, funding acquisition and conceptualization.

Acknowledgments

This work was funded by national funds through the Portuguese Foundation for Science and Technology (FCT) under FunFibRAI project with reference PTDC/EME-EME/4197/2021 (https://doi.org/10.54499/PTDC/EME-EME/4197/2021). Sara Madeira thanks FCT for the contract under the Stimulus of Scientific Employment 2023.08614.CEECIND/CP2841/CT0009 (https://doi.org/10.54499/2023.08614.CEECIND/CP2841/CT0009). This research was also funded by FCT through the project UID/04436: CMEMS-UMinho (https://doi.org/10.54499/UID/04436/2025). Flávio Rodrigues thanks FCT for PhD fellowship with reference 2023.05138.BDANA (https://doi.org/10.54499/2023.05138.BDANA). Diana P. Ferreira and Diego Chaves are thankful to the European Regional Development Fund (ERDF) through the Operational Competitiveness Program and the National Foundation for Science and Technology of Portugal (FCT) under the projects UID/CTM/00264/2020 of Centre for Textile Science and Technology (2C2T) on its components Base (https://doi.org/10.54499/UIDB/00264/2020) and programmatic (https://doi.org/10.54499/UIDP/00264/2020). Open access publication funding provided by FCT (b-on).

Funding

This work was funded by national funds through the Portuguese Foundation for Science and Technology (FCT) under the scope of the FunFibRAI project with reference PTDC/EME-EME/4197/2021 (https://doi.org/10.54499/PTDC/EME-EME/4197/2021). S. Madeira thanks FCT for the contract under the Stimulus of Scientific Employment 2023.08614.CEECIND/CP2841/CT0009 (https://doi.org/10.54499/2023.08614.CEECIND/CP2841/CT0009). This research was also funded by FCT through the project https://doi.org/10.54499/UID/04436/2025: CMEMS-UMinho. Flavio Rodrigues thanks FCT for PhD fellowship with reference 2023.05138.BDANA, https://doi.org/10.54499/2023.05138.BDANA. Diana Ferreira and Diego Chaves are thankful to the European Regional Development Fund (ERDF) through the Operational Competitiveness Program and the National Foundation for Science and Technology of Portugal (FCT) under the projects UID/CTM/00264/2020 of Centre for Textile Science and Technology (2C2T) on its components Base (https://doi.org/10.54499/UIDB/00264/2020) and programmatic (https://doi.org/10.54499/UIDB/00264/2020).

Conflicts of Interest

The authors declare no conflicts of interest.

Data Availability Statement

The data that support the findings of this study are available from the corresponding author upon reasonable request.

References

1. N. Jain, U. Dutt, I. Radenkov, and S. Jain, "WHO'S Global Oral Health Status Report 2022: Actions, Discussion and Implementation," *Oral Diseases* 30 (2024): 73–79.

2. G. Roberto and M. Matos, "Surface Roughness of Dental Implant and Osseointegration," *Journal of Maxillofacial and Oral Surgery* 20, no. 1 (2021): 1–4.

3. Y. Chee, "Retrospective Clinical Study on Survival Rate of Osseointegrated Dental Implants in the Early Post," *Clinical Oral Implants Research* 30 (2019): 369.

4. P. Bajaj, U. Shirbhate, and S. Dare, "Ligaplants: Uprising Regimen in the Glebe of Implant Dentistry," *Cureus* 15 (2023): e45968.

5. M. Saleem, M. Kaushik, A. Ghai, N. Tomar, and S. Singh, "Ligaplants: A Revolutionary Concept in Implant Dentistry," *Annals of Maxillofacial Surgery* 10, no. 1 (2020): 195–197.

6. L. P. Webber, H. L. Chan, and H. L. Wang, "Will Zirconia Implants Replace Titanium Implants?," *Applied Sciences* 11 (2021): 6776.

7. K. Sivaraman, A. Chopra, A. I. Narayan, and D. Balakrishnan, "Is Zirconia a Viable Alternative to Titanium for Oral Implant? A Critical Review," *Journal of Prosthodontic Research* 62 (2018): 121–133.

8. K. Shahramian, M. Gasik, I. Kangasniemi, et al., "Zirconia Implants With Improved Attachment to the Gingival Tissue," *Journal of Periodontology* 91 (2020): 1213–1224.

9. M. A. Saghiri, A. Asatourian, F. Garcia-Godoy, and N. Sheibani, "The Role of Angiogenesis in Implant Dentistry Part I: Review of Titanium Alloys, Surface Characteristics and Treatments," *Medicina Oral, Patología Oral y Cirugía Bucal* 21 (2016): e514.

10. R. Staples, S. Ivanovski, K. Vaswani, and C. Vaquette, "Melt Electrowriting Scaffolds With Fibre-Guiding Features for Periodontal Attachment," *Acta Biomaterialia* 180 (2024): 337–357.

11. R. Staples, S. Ivanovski, and C. Vaquette, "Fibre-Guiding Biphasic Scaffold for Perpendicular Periodontal Ligament Attachment," *Acta Biomaterialia* 150 (2022): 221–237.

12. S. Abraham, P. Gupta, K. Govarthanan, S. Rao, and T. S. Santra, "Direction-Oriented Fiber Guiding With a Tunable Tri-Layer-3D Scaffold for Periodontal Regeneration," *Royal Society of Chemistry* 14 (2024): 19806–19822.

13. A. Daghrery, J. A. Ferreira, I. J. de Souza Araújo, et al., "A Highly Ordered, Nanostructured Fluorinated CaP-Coated Melt Electrowritten Scaffold for Periodontal Tissue Regeneration," *Advanced Healthcare Materials* 10 (2021): 10.

14. C. H. Lee, J. Hajibandeh, T. Suzuki, A. Fan, P. Shang, and J. J. Mao, "Three-Dimensional Printed Multiphase Scaffolds for Regeneration of Periodontium Complex," *Tissue Engineering. Part A* 20 (2014): 1342–1351.

15. M. Olaru, L. Sachelarie, and G. Calin, "Hard Dental Tissues Regeneration-Approaches and Challenges," *Materials* 14 (2021): 14.

16. E. M. Varoni, S. Vijayakumar, E. Canciani, et al., "Chitosan-Based Trilayer Scaffold for Multitissue Periodontal Regeneration," *Journal of Dental Research* 97 (2018): 303–311.

17. K. Washio, Y. Tsutsumi, Y. Tsumanuma, et al., "In Vivo Periodontium Formation Around Titanium Implants Using Periodontal Ligament Cell Sheet," *Tissue Engineering. Part A* 24, no. 15–16 (2018): 1273–1282.

18. B. Choi, "Periodontal Ligament Formation Around Titanium Implants Using Cultured Periodontal Ligament Cells: A Pilot Study," *International Journal of Oral & Maxillofacial Implants* 15, no. 2 (2000): 193–196.

19. L. Sun and G. Hong, "Surface Modifications for Zirconia Dental Implants: A Review," *Frontiers in Dental Medicine* 2 (2021): 733242.

20. S. Roedel, J. Mesquita-Guimarães, J. C. M. Souza, F. S. Silva, M. C. Fredel, and B. Henriques, "Production and Characterization of Zirconia Structures With a Porous Surface," *Materials Science and Engineering C* 101 (2019): 264–273.

21. M. Proença, J. Ribeiro, P. Pinto, et al., "Channel-Embedded Porous Zirconia Surfaces to Mimic Dentine-Cementum Functionality in Dental Implants: Design, Production and Characterisation," *Ceramics International* 51 (2025): 48281–48294.

22. N. Juntavee, A. Juntavee, and P. Plongniras, "Remineralization Potential of Nano-Hydroxyapatite on Enamel and Cementum Surrounding Margin of Computer-Aided Design and Computer-Aided Manufacturing Ceramic Restoration," *International Journal of Nanomedicine* 13 (2018): 2755–2765.

23. S. Metwally and U. Stachewicz, "Teeth Resorption at Cement—Enamel Junction (CEJ)—Microscopy Analysis," *Micron* 137 (2020): 102913.

24. K. Sarna-Boś, K. Skic, P. Boguta, A. Adamczuk, M. Vodanovic, and R. Chałas, "Elemental Mapping of Human Teeth Enamel, Dentine and Cementum in View of Their Microstructure," *Micron* 172 (2023): 103485.

25. N. Nicklisch, C. Hinrichs, L. Palaske, W. Vach, and K. W. Alt, "Variability in Human Tooth Cementum Thickness Reflecting Functional Processes," *Journal of Periodontal Research* 59 (2024): 408–419.

26. X. Wen, F. Pei, Y. Jin, and Z. Zhao, "Exploring the Mechanical and Biological Interplay in the Periodontal Ligament," *International Journal of Oral Science* 17 (2025): 23.

27. A. Zaeri, K. Cao, F. Zhang, R. Zgeib, and R. C. Chang, "A Review of the Structural and Physical Properties That Govern Cell Interactions With Structured Biomaterials Enabled by Additive Manufacturing," *Bioprinting* 26 (2022): e00201.

28. Q. Hassan, S. Ahmadi, and K. Kerman, "Recent Advances in Monitoring Cell Behavior Using Cell-Based Impedance Spectroscopy," *Micromachines* 11 (2020): 590.

29. Y. Xu, X. Xie, Y. Duan, L. Wang, Z. Cheng, and J. Cheng, "A Review of Impedance Measurements of Whole Cells," *Biosensors & Bioelectronics* 77 (2016): 824–836.

30. D. D. Stupin, E. A. Kuzina, A. A. Abelit, et al., "Bioimpedance Spectroscopy: Basics and Applications," *ACS Biomaterials Science & Engineering* 7 (2021): 1962–1986.

31. K. Krukiewicz, "Electrochemical Impedance Spectroscopy as a Versatile Tool for the Characterization of Neural Tissue: A Mini Review," *Electrochemistry Communications* 116 (2020): 106742.

32. A. Bordbar-Khiabani and M. Gasik, "Electrochemical Behavior of Additively Manufactured Patterned Titanium Alloys Under Simulated Normal, Inflammatory, and Severe Inflammatory Conditions," *Journal of Materials Research and Technology* 26 (2023): 356–370.

33. A. Bordbar-Khiabani and M. Gasik, "Electrochemical and Biological Characterization of Ti–Nb–Zr–Si Alloy for Orthopedic Applications," *Scientific Reports* 13 (2023): 2312.

34. H. T. Ngoc Le, J. Kim, J. Park, and S. Cho, "A Review of Electrical Impedance Characterization of Cells for Label-Free and Real-Time Assays," *BioChip Journal* 13 (2019): 295–305.

35. M. Mour, D. Das, T. Winkler, et al., "Advances in Porous Biomaterials for Dental and Orthopaedic Applications," *Materials* 3 (2010): 2947–2974.

36. Y. Yao, J. E. Raymond, F. Kauffmann, et al., "Multicompartmental Scaffolds for Coordinated Periodontal Tissue Engineering," *Journal of Dental Research* 101 (2022): 1457–1466.

37. J. H. Nam, S. Y. Lee, G. Khan, and E. S. Park, "Validation of the Optimal Scaffold Pore Size of Nasal Implants Using the 3-Dimensional Culture Technique," *Archives of Plastic Surgery* 47 (2020): 310–316.

38. F. Mukasheva, L. Adilova, A. Dyussenbinov, B. Yernaimanova, M. Abilev, and D. Akilbekova, "Optimizing Scaffold Pore Size for Tissue Engineering: Insights Across Various Tissue Types," *Frontiers in Bioengineering and Biotechnology* 12 (2024): 1444986.

39. S. Deville, "Freeze-Casting of Porous Biomaterials: Structure, Properties and Opportunities," *Materials* 3 (2010): 1913–1927.

40. J. Chevalier, "What Future for Zirconia as a Biomaterial?," *Biomaterials* 27 (2006): 535–543.

41. P. Lekic and C. A. G. Mcculloch, "Periodontal Ligament Cell Populations: The Central Role of Fibroblasts in Creating a Unique Tissue," *Anatomical Record* 245 (1996): 327–341.

42. Y. Huang, Y. Tang, R. Zhang, et al., "Role of Periodontal Ligament Fibroblasts in Periodontitis: Pathological Mechanisms and Therapeutic Potential," *Journal of Translational Medicine* 22 (2024): 1136.

43. T. Jin, "Gradient Sensing During Chemotaxis," *Current Opinion in Cell Biology* 25 (2013): 532–537.

44. X. Dolde, C. Karreman, M. Wiechers, S. Schildknecht, and M. Leist, "Profiling of Human Neural Crest Chemoattractant Activity as a Replacement of Fetal Bovine Serum for In Vitro Chemotaxis Assays," *International Journal of Molecular Sciences* 22 (2021): 10079.

45. L. M. Santos, P. E. S. Cardoso, E. A. Diniz, J. G. Rahhal, and C. R. Sipert, "Different Concentrations of Fetal Bovine Serum Affect Cytokine Modulation in Lipopolysaccharide-Activated Apical Papilla Cells In Vitro," *Journal of Applied Oral Science* 31 (2023): e20230020.

46. X. Zheng, H. Baker, W. S. Hancock, F. Fawaz, M. McCaman, and E. Pungor, "Proteomic Analysis for the Assessment of Different Lots of Fetal Bovine Serum as a Raw Material for Cell Culture. Part IV. Application of Proteomics to the Manufacture of Biological Drugs," *Biotechnology Progress* 22 (2006): 1294–1300.

47. D. Kwon, J. S. Kim, B. H. Cha, et al., "The Effect of Fetal Bovine Serum (FBS) on Efficacy of Cellular Reprogramming for Induced Pluripotent Stem Cell (iPSC) Generation," *Cell Transplantation* 25 (2016): 1025–1042.

48. C. R. Pilgrim, K. A. McCahill, J. G. Rops, J. M. Dufour, K. A. Russell, and T. G. Koch, "A Review of Fetal Bovine Serum in the Culture of Mesenchymal Stromal Cells and Potential Alternatives for Veterinary Medicine," *Frontiers in Veterinary Science* 9 (2022): 9.

49. T. Yang, Y. Li, Y. Hong, et al., "The Construction of Biomimetic Cementum Through a Combination of Bioskiving and Fluorine-Containing Biomineralization," *Frontiers in Bioengineering and Biotechnology* 8 (2020): 533175.

50. R. R. Khasawneh, A. H. Al Sharie, E. Abu-El Rub, A. O. Serhan, and H. N. Obeidat, "Addressing the Impact of Different Fetal Bovine Serum Percentages on Mesenchymal Stem Cells Biological Performance," *Molecular Biology Reports* 46 (2019): 4437–4441.

51. T. Yurube, W. J. Buchser, H. J. Moon, et al., "Serum and Nutrient Deprivation Increases Autophagic Flux in Intervertebral Disc Annulus Fibrosus Cells: An In-Vitro Experimental Study," *European Spine Journal* 28 (2019): 993.

52. F. Boraldi, G. Annovi, C. Paolinelli-Devincenzi, R. Tiozzo, and D. Quaglino, "The Effect of Serum Withdrawal on the Protein Profile of Quiescent Human Dermal Fibroblasts in Primary Cell Culture," *Proteomics* 8 (2008): 66–82.

53. T. Lebedev, A. Mikheeva, V. Gasca, P. Spirin, and V. Prassolov, "Systematic Comparison of FBS and Medium Variation Effect on Key Cellular Processes Using Morphological Profiling," *Cells* 14 (2025): 336.

54. H. Harianawala, M. Kheur, S. Kheur, et al., "Biocompatibility of Zirconia," *Journal of Advanced Medical and Dental Sciences Research* 4 (2016): 35–39.

55. P. V. Singh, A. Reche, P. Paul, and S. Agarwal, "Zirconia Facts and Perspectives for Biomaterials in Dental Implantology," *Cureus* 15 (2023): e46828.

56. M. B. da Cruz, J. F. Marques, N. Silva, et al., "Human Gingival Fibroblast and Osteoblast Behavior on Groove-Milled Zirconia Implant Surfaces," *Materials* 15 (2022): 15.

57. Y. D. Cho, J. C. Shin, H. I. Yoon, et al., "Characterization of Human Gingival Fibroblasts on Zirconia Surfaces Containing Niobium Oxide," *Materials* 8 (2015): 6018.

58. M. G. Sghaireen, M. R. Alrwuili, N. A. Alenzi, M. A. Aljabab, R. Issrani, and M. K. Alam, "Analysis of the Cellular Response to Different Dental Implant Surfaces: An In Vitro Study," *Journal of Pharmacy & Bioallied Sciences* 16 (2024): S2521–S2523.

59. W. M. S. Al Qahtani, C. Schille, S. Spintzyk, et al., "Effect of Surface Modification of Zirconia on Cell Adhesion, Metabolic Activity and Proliferation of Human Osteoblasts," *Biomedizinische Technik* 62 (2017): 75–87.

60. A. Samourides, L. Browning, V. Hearnden, and B. Chen, "The Effect of Porous Structure on the Cell Proliferation, Tissue Ingrowth and Angiogenic Properties of Poly(Glycerol Sebacate Urethane) Scaffolds," *Materials Science and Engineering C* 108 (2020): 110384.

61. S. Y. Lee, T. Fujioka, M. Osuga, T. Nishimura, and S. Suetsugu, "Lamellipodia and Filopodia," in *Plasma Membrane Shaping* (Academic Press, 2023), 245–263.

62. N. Leijnse, Y. F. Barooji, M. R. Arastoo, et al., "Filopodia Rotate and Coil by Actively Generating Twist in Their Actin Shaft," *Nature Communications* 13 (2022): 13.

63. W. Gamal, H. Wu, I. Underwood, J. Jia, S. Smith, and P. O. Bagnaninchi, "Impedance-Based Cellular Assays for Regenerative Medicine," *Philosophical Transactions of the Royal Society, B: Biological Sciences* 373 (2018): 20170226.

64. M. Hernández, M. A. Álvarez-Pérez, J. Genesca, K. K. Gómez, and A. Covelo, "Evaluation of the Biocompatibility of a PVA/SA Scaffold With a Human Gingival Fibroblast (HGF) by Using Electrochemical Impedance Spectroscopy," *Bioelectrochemistry* 131 (2020): 107386.

65. C. Pitsalidis, D. Van Niekerk, C. M. Moysidou, et al., "Organic Electronic Transmembrane Device for Hosting and Monitoring 3D Cell Cultures," *Science Advances* 8 (2022): eabo4761.

66. A. Kociubiński, "Electric Cell-Substrate Impedance Sensing in Biocompatibility Research," *Journal of Electrical Bioimpedance* 12 (2021): 163–168.

67. R. C. Nordberg, J. Zhang, E. H. Griffith, M. W. Frank, B. Starl, and E. G. Loboa, "Electrical Cell-Substrate Impedance Spectroscopy Can Monitor Age-Grouped Human Adipose Stem Cell Variability During Osteogenic Differentiation," *Stem Cells Translational Medicine* 6, no. 2 (2017): 502–511.

68. R. Ramos, K. Zhang, D. Quinn, S. W. Sawyer, S. Mcloughlin, and P. Soman, "Measuring Changes in Electrical Impedance During Cell-Mediated Mineralization," *Bioelectricity* 1 (2019): 73–84.